AIAA JOURNAL
Vol. 45, No. 9, September 2007

Micromechanical Analysis of Composite Corrugated-Core Sandwich Panels for Integral Thermal Protection Systems

Oscar A. Martinez,* Bhavani V. Sankar,† Raphael T. Haftka,‡ and Satish K. Bapanapalli§
University of Florida, Gainesville, Florida 32611
and
Max L. Blosser¶
NASA Langley Research Center, Hampton, Virginia 23681

DOI: 10.2514/1.26779

A composite corrugated-core sandwich panel was investigated as a potential candidate for an integral thermal protection system. This multifunctional integral thermal protection system concept can protect the space vehicle from extreme reentry temperatures, and possess load-carrying capabilities. The corrugated core is composed of two, thin, flat sheets that are separated by two inclined plates. Advantages of this new integral thermal protection system concept are discussed. The sandwich structure is idealized as an equivalent orthotropic thick-plate continuum. The extensional stiffness matrix [A], coupling stiffness matrix [B], bending stiffness [D], and the transverse shear stiffness terms A_{44} and A_{55} were calculated using an energy approach. Using the shear-deformable plate theory, a closed-form solution of the plate response was derived. The variation of plate stiffness and maximum plate deflection due to changing the web angle are discussed. The calculated results, which require significantly less computational effort and time, agree well with the three-dimensional finite element analysis. This study indicates that panels with rectangular webs resulted in a weak extensional, bending, and A_{55} stiffness and that the center plate deflection was minimum for a triangular corrugated core. The micromechanical analysis procedures developed in this study were used to determine the stresses in each component of the sandwich panel (face and web) due to a uniform pressure load.

Nomenclature

a	=	panel length, x direction
b	=	panel width, y direction
d	=	height of the sandwich panel (centerline to centerline)
$\{\boldsymbol{D}\}^{(e)}$	=	deformation vector of the eth component (microdeformation)
$\{\boldsymbol{D}\}^{M}$	=	deformation vector of the unit cell (macrodeformation)
e	=	component index of the unit cell
$F_i^{(m)}$	=	nodal force in the finite element method model
l	=	length of the cantilever beam
P_z	=	pressure load acting on the two-dimensional orthotropic panel
Q_x, Q_y	=	shear force on the unit cell
Q_{ij}	=	transformed lamina stiffness matrix
s	=	web length
$[T_D]^{(e)}$	=	deformation transformation matrix of the ith component of the corrugated core
t_{TF}	=	top face sheet thickness
t_{BF}	=	bottom face sheet thickness
t_w	=	web thickness
U	=	unit-cell strain energy
w	=	integral thermal protection system panel deflection
$\bar{y}$	=	local axis of the web
ε_o	=	midplane strain
θ	=	angle of web inclination
κ	=	curvature
$\tau_{\overline{xy}}$	=	shear stress in the web
ψ_x, ψ_y	=	rotations of the plate's cross section
$2p$	=	unit-cell length

Presented as Paper 1876 at the 47th AIAA/ASME/ASCE/AHS/ASC Structures, Structural Dynamics, and Materials Conference, Newport, Rhode Island, 1–4 May 2006; received 7 August 2006; revision received 16 March 2007; accepted for publication 17 April 2007.

*Department of Mechanical and Aerospace Engineering, Graduate Student.
†Newton C. Ebaugh Professor, Department of Mechanical and Aerospace Engineering. AIAA Associate Fellow.
‡Distinguished Professor, Department of Mechanical and Aerospace Engineering. AIAA Fellow.
§Graduate Student, Department of Mechanical and Aerospace Engineering.
¶Aerospace Technologist, NASA Langley Research Center.

I. Introduction

REDUCING the cost of launching a space vehicle into space is one of the critical needs of the space industry. Government and private corporations use space for various objectives, such as reconnaissance, communications, weather-monitoring, military, and other experimental purposes. One of NASA's goals is to reduce the cost of delivering a pound of payload into space by an order of magnitude [1]. The space vehicle's thermal protection system (TPS) is one of the most expensive and critical systems of the vehicle [2]. Future space vehicles require more advanced TPS than the one currently used. The main function of the TPS is to protect the space vehicle from the extreme aerodynamic heating during planetary reentry. The TPS is the key feature that makes a space vehicle lightweight, fully reusable, and easily maintainable.

The space shuttle's current TPS technology consists of different types of materials such as ceramic tiles and blankets which are distributed all over the spacecraft. This technology makes the space vehicles' exterior very brittle, susceptible to damage from small impact loads, and high in maintenance time and cost. To overcome these difficulties, scientists at NASA developed a metallic TPS called ARMOR TPS [3,4]. However, the ARMOR TPS's load-bearing capabilities are limited and large in-plane loads cannot be accommodated under this design. A common feature of the Space Shuttle's TPS system and the ARMOR TPS system is that they are all

attached to the space vehicle. Currently the TPS on the Space Shuttle requires 40,000 man-hours of maintenance between typical flights [1] because it is an add-on feature.

The new TPS concept presented in this article can be accomplished by using recently developed metallic foams and also innovative core materials, such as corrugated and truss cores. The integral TPS/structure (ITPS) design can significantly reduce the overall weight of the vehicle as the TPS/structure performs the load-bearing and thermal function. Sandwich structures can offer high stiffness with relatively much weight saving when compared with widely used laminated structures. They also possess good vibration characteristics when compared with thin plate-like structures. Sandwich structures have good damage tolerance properties and can withstand small object impact.

Fung et al. [5,6] and Libove and Hubka [7] used the equivalent homogenous model approach and force-distortion relationship to derive the elastic constants of Z-core, C-core, and corrugated-core sandwich panels. More recently developed truss-core sandwich panels have been investigated by Lok and Cheng [8] and Valdevit et al. [9]. Lok et al. [10] and Valdevit et al. [9] investigated and analyzed metallic corrugated-core sandwich panels. Lok et al. [8,10] derived analytical equations using the force-distortion relationships of an orthotropic thick plate to predict the elastic stiffness properties and behavior of truss-core sandwich panels. The researchers used the homogenous equivalent thick-plate approach to represent the three-dimensional structure into a two-dimensional orthotropic plate. The researchers verified and compared their results with finite element analyses and conventional sandwich forms that were investigated by Libove et al. [11,12].

Composite corrugated-core sandwich structures will be investigated in this paper for use in multifunctional structures for future space vehicles (Fig. 1). This type of ITPS would insulate the vehicle from aerodynamic heating as well as carry primary vehicle loads. The advantages of using such a structure is that it has the potential of being lightweight because of the thin faces and corrugation feature. The structure offers insulation as well as load-bearing capabilities which makes it multifunctional. The panels can be large in size thus reducing the number of panels needed. Integration with the space vehicle promotes low maintenance. The corrugated-core sandwich panel is composed of several unit cells. The unit cell consists of two thin face sheets and an inclined web, which can be of homogeneous materials such as metals or composite laminates. The composite corrugated core will be filled with Saffil, which is a non-load-bearing insulation made of alumina fibers.

This paper's objective is to determine the equivalent stiffness properties of the ITPS panel by idealizing it as a continuum. The extensional stiffness matrix [A], coupling stiffness matrix [B], bending stiffness [D], and the transverse shear stiffness terms A_{44} and A_{55} were calculated by analyzing the unit cell. A detailed formulation and description of the extensional, coupling, bending, and shearing stiffness of the ITPS panel are presented for a unit cell by representing the sandwich panel as an equivalent thick plate, which is homogeneous, continuous, and orthotropic with respect to the x and y directions. A strain-energy approach and a deformation transformation matrix were used in deriving the analytical equations of the equivalent extensional, bending, coupling, and shearing stiffnesses. Previous researchers adopted the force-distortion relationship approach to determine the equivalent stiffness parameters. The force-distortion relationship approach becomes complicated and tedious if the ITPS is composed of faces and webs with different materials and thickness. This problem can be solved with the proposed strain-energy approach and deformation transformation matrix. The stiffness results are used in the first order shear-deformable plate theory (FSDT) to determine the response of an ITPS plate when subjected to mechanical and thermal loads. The analytical models are compared with detailed finite element analysis.

II. Geometric Parameters

Consider a simplified geometry of the corrugated-core unit cell in Fig. 2. The z axis is in the thickness direction of the ITPS panel. The stiffer longitudinal direction is parallel to the x axis, and the y axis is in the transverse direction. The unit cell consists of two inclined webs and two thin face sheets. The unit cell is symmetric with respect to the yz plane. The upper face plate thickness t_{TF} can be different from the lower plate thickness t_{TB} as well as the web thickness t_w. The unit cell can be identified by six geometric parameters ($p, d, t_{\mathrm{TF}}, t_{\mathrm{BF}}, t_w, \theta$) (Fig. 2). Four other dimensions (b_c, d_c, s, f) are obtained from geometric considerations. The equations for these relationships are as follows:

$$d_c = d - \frac{1}{2}t_{\mathrm{TF}} - \frac{1}{2}t_{\mathrm{BF}} \tag{1a}$$

$$f = \frac{1}{2}\left(p - \frac{d_c}{\tan\theta}\right) \tag{1b}$$

$$b_c = p - 2f \tag{1c}$$

$$s = \sqrt{d_c^2 + b_c^2} = \frac{d_c}{\sin\theta} = \frac{b_c}{\cos\theta} \tag{1d}$$

The ratio $f/p = 0$ corresponds to a triangular core and $f/p = 0.5$ corresponds to a rectangular core.

III. Analysis

The finite element method (FEM) is commonly used to analyze sandwich structures. Shell elements are often preferred for the faces and webs to construct a three-dimensional FEM model. However, the number of elements and nodes needed to appropriately mesh the sandwich panel can be excessive; as a result, a three-dimensional FEM model is not economical for a quick preliminary analysis of an ITPS. Such panels may also be represented as a thick plate that is continuous, orthotropic, and homogenous for which analytical and two-dimensional FEM solutions [13] are available.

The extensional stiffness matrix [A], coupling stiffness matrix [B], bending stiffness [D], and the transverse shear stiffness terms A_{44} and A_{55} are calculated by analyzing the unit cell. For bending analysis of the plate, a closed-form solution was obtained by using the FSDT. Advanced knowledge of the orthotropic thick-plate stiffness is

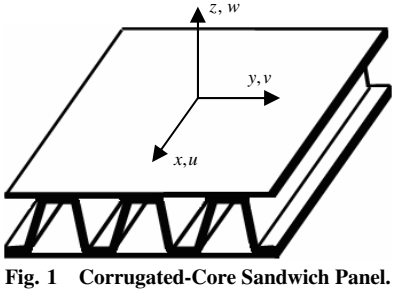

Fig. 1 Corrugated-Core Sandwich Panel.

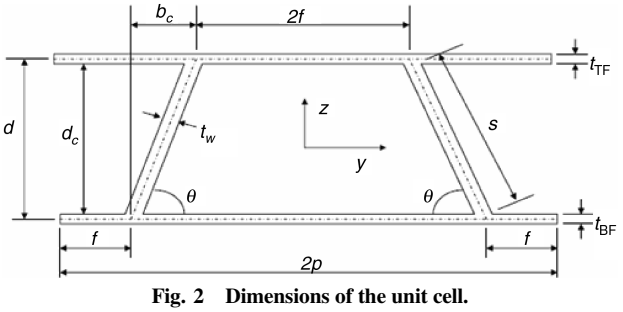

Fig. 2 Dimensions of the unit cell.

essential for successful implementation of the FSDT. Typically, plate analyses yield information on deflections, and force and moment resultants at any point on the plate. We will again use the micromechanical analysis procedures developed in this study to determine the local stresses in the face sheets and the webs. Then failure theories such as Tsai–Hill criterion can be used to determine if the stresses are acceptable or not.

In the derivation of the stiffness parameters, the following assumptions were made:

1) The deformation of the panel is small when compared with the panel thickness.

2) The panel dimensions in the x direction are much larger than the unit-cell width $2p$.

3) The face sheets are thin with respect to the core thickness.

4) The core contributes to bending stiffness in and about the x axis but not about the y axis.

5) The face and web laminates are symmetric with respect to their own midplanes.

6) The core is sufficiently stiff so that the elastic modulus in the z direction is assumed to be infinite for the equivalent plate. Local buckling of the facing plates does not occur and the overall thickness of the panel is constant.

Previous researchers adopted these assumptions in the derivation of stiffness parameters of sandwich panels with corrugated core; Libove and Hubka [7] for C-core, and Fung et al. for Z-core [5,6]. The in-plane and out-of-plane stiffness governing the elastic response of a shear-deformable sandwich panel are defined in the context of laminated plate theory incorporating FSDT described by Vinson [14] and Whitney [15]. The appropriate stiffness of the orthotropic plate may be obtained by comparing the behavior of a unit cell of the corrugated-core sandwich panel with that of an element of the idealized homogeneous orthotropic plate (Fig. 3).

The in-plane extensional and shear response and out-of-plane (transverse) shear response of an orthotropic panel are governed by the following constitutive relation:

$$\begin{bmatrix} N \\ Q \\ M \end{bmatrix} = \begin{bmatrix} [A] & & \\ & [C] & \\ & & [D] \end{bmatrix} \begin{Bmatrix} \varepsilon_o \\ \gamma \\ \kappa \end{Bmatrix} \quad \text{or} \quad \{F\} = [K]\{\boldsymbol{D}\} \tag{2}$$

In Eq. (2), ε and γ are the normal and shear strains, κ are the bending and twisting curvatures, and [A], [C], and [D] are the extensional, shear, and bending stiffness. The orthotropic plate is assumed to be symmetric.

A. Extensional and Bending Stiffness

An analytical method was developed to calculate the stiffness matrix of the corrugated-core sandwich panel. Consider a unit cell made up of four composite laminates (two face sheets and two webs). Each laminate has its respective material properties and *ABD* matrix. The *ABD* matrix of each component needs to be combined together in an appropriate manner to create the overall stiffness of the sandwich panel. The formulas for determining the *ABD* matrix of a composite laminate are given as follows [16]:

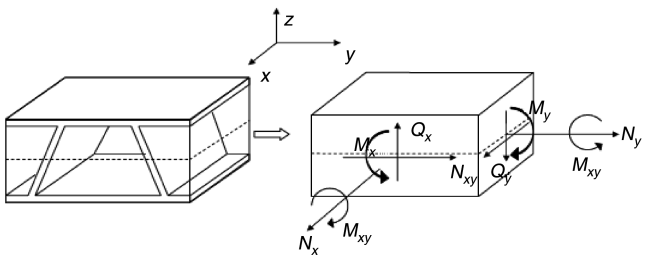

Fig. 3 Equivalent orthotropic thick plate for the unit-cell corrugated-core sandwich panel.

$$\left[A_{ij}^e, B_{ij}^e, D_{ij}^e\right] = \int_{-\frac{t}{2}}^{\frac{t}{2}} \left(\bar{Q}_{ij}^e\right)_k [1, z, z^2]\,\mathrm{d}z$$

$$= \sum_{k=1}^{N} \left(\bar{Q}_{ij}^e\right)_k \left[(z_k - z_{k-1}), \frac{\left(z_k^2 - z_{k-1}^2\right)}{2}, \frac{\left(z_k^3 - z_{k-1}^3\right)}{3}\right] \tag{3}$$

In Eq. (3), N is the number of laminas in the composite and Q_{ij}^e are the components of the transformed lamina stiffness matrix, where $e = 1$–4 (1 = top face sheet, 2 = bottom face sheet, 3 = left web, 4 = right web). The overall stiffness of the unit cell was determined by imposing unit midplane strains and curvatures (macrodeformation) to the unit cell and then calculating the corresponding midplane strains and curvatures (microdeformations) in each component. The unit-cell components are the two face sheets and two webs. A transformation matrix relates the macro- and microdeformations as follows:

$$\{\boldsymbol{D}\}^{(e)} = [T_D]^{(e)}\{\boldsymbol{D}\}^M \tag{4}$$

In Eq. (4), $\{\boldsymbol{D}\}^{(e)}$ is the microdeformation in each component, $\{\boldsymbol{D}\}^M$ is the macrodeformation of the unit cell, and $T_D^{(e)}$ is the deformation transformation matrix that relates macrodeformation to microdeformations.

B. Formulation of Deformation Transformation Matrix Face Sheets

The deformation transformation matrix of the top face sheet was determined by first considering the unit cell under the action of midplane macrostrains ε_{xo}, ε_{yo}, γ_{xyo} and macrocurvature κ_x, κ_y, κ_{xy}. Each strain and curvature was considered by itself and the resulting midplane strains and curvatures in the face sheets (also known as microstrains and curvatures) were derived. The following equations show the transformation matrices of the top and bottom face sheets.

Top face sheet

$$\{\boldsymbol{D}\}^{(1)} = T_D^1\{\boldsymbol{D}\}^M$$

$$\begin{Bmatrix} \varepsilon_{xo} \\ \varepsilon_{yo} \\ \gamma_{xyo} \\ \kappa_x \\ \kappa_y \\ \kappa_{xy} \end{Bmatrix}^{(1)} = \begin{bmatrix} 1 & 0 & 0 & \frac{d}{2} & 0 & 0 \\ 0 & 1 & 0 & 0 & \frac{d}{2} & 0 \\ 0 & 0 & 1 & 0 & 0 & \frac{d}{2} \\ 0 & 0 & 0 & 1 & 0 & 0 \\ 0 & 0 & 0 & 0 & 1 & 0 \\ 0 & 0 & 0 & 0 & 0 & 1 \end{bmatrix} \begin{Bmatrix} \varepsilon_{xo} \\ \varepsilon_{yo} \\ \gamma_{xyo} \\ \kappa_x \\ \kappa_y \\ \kappa_{xy} \end{Bmatrix}^{(M)} \tag{5}$$

Bottom face sheet

$$\{\boldsymbol{D}\}^{(2)} = T_D^2\{\boldsymbol{D}\}^M$$

$$\begin{Bmatrix} \varepsilon_{xo} \\ \varepsilon_{yo} \\ \gamma_{xyo} \\ \kappa_x \\ \kappa_y \\ \kappa_{xy} \end{Bmatrix}^{(1)} = \begin{bmatrix} 1 & 0 & 0 & -\frac{d}{2} & 0 & 0 \\ 0 & 1 & 0 & 0 & -\frac{d}{2} & 0 \\ 0 & 0 & 1 & 0 & 0 & -\frac{d}{2} \\ 0 & 0 & 0 & 1 & 0 & 0 \\ 0 & 0 & 0 & 0 & 1 & 0 \\ 0 & 0 & 0 & 0 & 0 & 1 \end{bmatrix} \begin{Bmatrix} \varepsilon_{xo} \\ \varepsilon_{yo} \\ \gamma_{xyo} \\ \kappa_x \\ \kappa_y \\ \kappa_{xy} \end{Bmatrix}^{(M)} \tag{6}$$

There is a 1:1 relationship between midplane macro- and microstrain as well as a 1:1 relationship between macro- and microcurvature, as indicated by unity along the diagonal of the transformation matrices. Using the assumptions that the in-plane displacements u and v are linear functions of the z coordinate and that the transverse normal strain ε_z is negligible [16], the $d/2$ factor was used to relate the macrocurvatures to the midplane microstrains.

C. Formulation of Deformation Transformation Matrix for the Webs

Formulation of the deformation transformation matrix for the webs is relatively complicated because of the need for coordinate transformation due to the inclination of the webs. Consider a global xyz coordinate system and a local $\overline{xyz}$ coordinate system (Fig. 4).

The origin of the local web axis is at the top face sheet and web junction point. The transformation from global to local coordinate axes requires a rotation and translation. The transformation from global to local displacements only requires a rotation (see Appendix A). In Eq. (A1), θ is the angle of web inclination of the right web, the first matrix is the rotation matrix, and the second vector is a translation vector. Consider the unit cell of the ITPS panel under the action of midplane macrostrains $\varepsilon_{xo}, \varepsilon_{yo}, \gamma_{xyo}$ and macrocurvature $\kappa_x, \kappa_y, \kappa_{xy}$. From Assumption 4 in Sec. III we noted that $\varepsilon_{\bar{y}o}^{(3,4)} = 0$ and $\varepsilon_{\bar{x}o}^{(3,4)} = 1$ when the unit cell is subjected to $\varepsilon_{yo}^{M} = 1$ and $\varepsilon_{xo}^{M} = 1$. The microstrains on the webs due to a macrocurvature are more complex to determine, therefore a detailed discussion is appropriate (see Appendix A). The microstrains and curvature in the right web due to a macrounit curvature along the y axis (κ_y) was derived; all other curvatures were set equal to zero.

$$\kappa_x = -\frac{\partial^2 w}{\partial x^2} = 0 \qquad \kappa_y = -\frac{\partial^2 w}{\partial y^2} = 1 = \kappa_o \qquad \kappa_{xy} = -2\frac{\partial^2 w}{\partial x \partial y} = 0 \tag{7}$$

Starting with Eq. (7) and following the detailed derivation in Appendix A leads to the transformation matrix for the left and right web.

Left web

$$\{\boldsymbol{D}\}^{(3)} = T_D^3\{\boldsymbol{D}\}^M \qquad \begin{Bmatrix} \varepsilon_{\bar{x}o} \\ \varepsilon_{\bar{y}o} \\ \gamma_{\overline{xy}o} \\ \kappa_{\bar{x}} \\ \kappa_{\bar{y}} \\ \kappa_{\overline{xy}} \end{Bmatrix}^{(3)} = \begin{bmatrix} 1 & 0 & 0 & \left(\frac{d_c}{2} - \bar{y}\sin\theta\right) & 0 & 0 \\ 0 & 0 & 0 & 0 & \cos^2\theta\left(\frac{d_c}{2} - \bar{y}\sin\theta\right) & 0 \\ 0 & 0 & -\cos\theta & 0 & 0 & -\cos\theta\left(\frac{d_c}{2} - \bar{y}\sin\theta\right) \\ 0 & 0 & 0 & -\cos\theta & 0 & 0 \\ 0 & 0 & 0 & 0 & -\cos^3\theta - 2\cos\theta\sin^2\theta & 0 \\ 0 & 0 & 0 & 0 & 0 & 1 \end{bmatrix} \begin{Bmatrix} \varepsilon_{xo} \\ \varepsilon_{yo} \\ \gamma_{xyo} \\ \kappa_x \\ \kappa_y \\ \kappa_{xy} \end{Bmatrix}^{(M)} \tag{8}$$

Right web

$$\{\boldsymbol{D}\}^{(4)} = T_D^4\{\boldsymbol{D}\}^M \qquad \begin{Bmatrix} \varepsilon_{\bar{x}o} \\ \varepsilon_{\bar{y}o} \\ \gamma_{\overline{xy}o} \\ \kappa_{\bar{x}} \\ \kappa_{\bar{y}} \\ \kappa_{\overline{xy}} \end{Bmatrix}^{(4)} = \begin{bmatrix} 1 & 0 & 0 & \left(\frac{d_c}{2} - \bar{y}\sin\theta\right) & 0 & 0 \\ 0 & 0 & 0 & 0 & \cos^2\theta\left(\frac{d_c}{2} - \bar{y}\sin\theta\right) & 0 \\ 0 & 0 & \cos\theta & 0 & 0 & \cos\theta\left(\frac{d_c}{2} - \bar{y}\sin\theta\right) \\ 0 & 0 & 0 & \cos\theta & 0 & 0 \\ 0 & 0 & 0 & 0 & \cos^3\theta + 2\cos\theta\sin^2\theta & 0 \\ 0 & 0 & 0 & 0 & 0 & 1 \end{bmatrix} \begin{Bmatrix} \varepsilon_{xo} \\ \varepsilon_{yo} \\ \gamma_{xyo} \\ \kappa_x \\ \kappa_y \\ \kappa_{xy} \end{Bmatrix}^{(M)} \tag{9}$$

From Eqs. (8) and (9) we observe that micromidplane strains in the webs are a linear function of $\bar{y}$.

D. Stiffness Matrix Determination Through Strain-Energy Approach

As the unit cell is deformed by the unit macrostrains and curvatures, it stores energy internally throughout its volume. The total strain energy in the unit cell is the sum of strain energies in the individual components, i.e., faces and webs.

$$U^M = \frac{1}{2}(2p)^2(\{\boldsymbol{D}\}^M)^T[K]\{\boldsymbol{D}\}^M = \sum_{e=1}^{4} U^{(e)} \tag{10}$$

In Eq. (10), U^M is the total strain energy and $U^{(e)}$ is the strain energy of the eth component. The strain energy of an individual component is shown in Eq. (11). Because the deformations of the webs are a function of $\bar{y}$, integration of Eq. (11) is done with respect to $\bar{y}$. The integration limits are from zero to s, where s is the length of the webs. By substituting Eq. (4) into Eq. (11) we are able to represent the strain energy of the web in terms of macrodeformations of the unit cell. In Eq. (11), $A^{(e)}$ denotes the area of the eth component.

$$U^{(e)} = \int_{A^{(e)}} \frac{1}{2}(\{\boldsymbol{D}\}^{(e)})^T[K]^{(e)}\{\boldsymbol{D}\}^{(e)}\,\mathrm{d}A^{(e)} \tag{11}$$

$$U^{(4)} = (2p)\int_0^s \frac{1}{2}(\{\boldsymbol{D}\}^{(4)})^T[K]^{(4)}\{\boldsymbol{D}\}^{(4)}\,\mathrm{d}\bar{y} \tag{12}$$

$$U^{(4)} = \frac{1}{2}(2p)\int_0^s (T_D^4\{\boldsymbol{D}\}^M)^T[K]^4(T_D^4\{\boldsymbol{D}\}^M)\,\mathrm{d}\bar{y} \tag{13}$$

In general, we write the strain energy in each laminate in terms of the global deformation $\{\boldsymbol{D}\}^M$ as

$$U^{(e)} = \frac{1}{2}(D^M)^T K^{(e)} D^M \tag{14}$$

Then the stiffness matrix K of the idealized orthotropic panel can be derived as

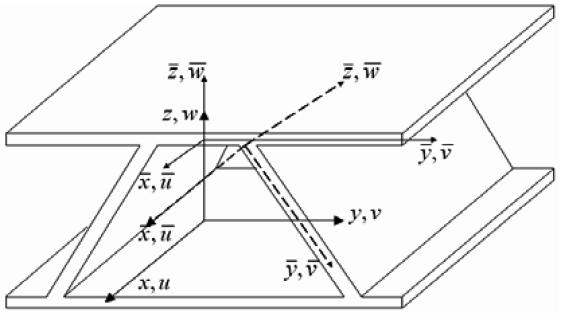

Fig. 4 Global and local coordinate axes for the right web.

$$K = \sum_{e=1}^{4} K^{(e)} = \frac{1}{2p} \sum_{e=1}^{4} \int_0^L (T_D^{(e)})^T [K]^{(e)} (T_D^{(e)})\, \mathrm{d}\bar{y} \tag{15}$$

E. Face and Web Stresses

It has been shown that using the deformation transformation matrix one can determine the local strains and curvature of each part of the unit cell (face or web) due to a unit-cell deformation. As a result of that, we obtained stresses in each component by multiplying the microdeformations and curvatures of a particular component with the corresponding transformed lamina stiffness matrix.

$$\begin{Bmatrix} \varepsilon_o \\ \kappa \end{Bmatrix}^{(e)} = [T_D]^{(e)} \begin{Bmatrix} \varepsilon_o \\ \kappa \end{Bmatrix}^{(M)} \tag{16}$$

$$[\sigma]^{(e)} = [\bar{Q}]^{(e)} (\{\varepsilon_o\}^{(e)} + z\{\kappa\}^{(e)}) \tag{17}$$

Although the previously derived deformation transformation matrices for the webs, Eqs. (8) and (9), are good for stiffness prediction, they do not yield accurate stress results when compared with finite element (FE) analysis. For example, the assumption $\varepsilon_z^M = 0$ constrains the webs from expanding in the $\bar{y}$ direction due to the Poisson effect. This leads to stresses in the $\bar{y}$ direction that are not present in the three-dimensional FE analysis. Therefore, corrections were applied to the deformation transformation matrix to obtain accurate web stresses. The refined web stress deformation transformation matrices for the webs are as follows.

Left web

$$\{\boldsymbol{D}\}^{(e)} = T_D^e \{\boldsymbol{D}\}^M \qquad \begin{Bmatrix} \varepsilon_{\bar{x}o} \\ \varepsilon_{\bar{y}o} \\ \gamma_{\overline{xy}o} \\ \kappa_{\bar{x}} \\ \kappa_{\bar{y}} \\ \kappa_{\overline{xy}} \end{Bmatrix}^{(3)} = \begin{bmatrix} 1 & 0 & 0 & \left(\frac{d_c}{2} - \bar{y}\sin\theta\right) & 0 & 0 \\ \nu & 0 & 0 & \nu\left(\frac{d_c}{2} - \bar{y}\sin\theta\right) & 0 & 0 \\ 0 & 0 & -f(p,d,t_{\mathrm{TF}},t_{\mathrm{BF}},t_w,\theta) & 0 & 0 & 0 \\ 0 & 0 & 0 & -\cos\theta & 0 & 0 \\ 0 & 0 & 0 & 0 & -g(p,d,t_{\mathrm{TF}},t_{\mathrm{BF}},t_w,\theta) & 0 \\ 0 & 0 & 0 & 0 & 0 & 1 \end{bmatrix} \begin{Bmatrix} \varepsilon_{xo} \\ \varepsilon_{yo} \\ \gamma_{xyo} \\ \kappa_x \\ \kappa_y \\ \kappa_{xy} \end{Bmatrix}^{(M)} \tag{18}$$

Right web

$$\{\boldsymbol{D}\}^{(e)} = T_D^e \{\boldsymbol{D}\}^M \qquad \begin{Bmatrix} \varepsilon_{\bar{x}o} \\ \varepsilon_{\bar{y}o} \\ \gamma_{\overline{xy}o} \\ \kappa_{\bar{x}} \\ \kappa_{\bar{y}} \\ \kappa_{\overline{xy}} \end{Bmatrix}^{(3)} = \begin{bmatrix} 1 & 0 & 0 & \left(\frac{d_c}{2} - \bar{y}\sin\theta\right) & 0 & 0 \\ \nu & 0 & 0 & \nu\left(\frac{d_c}{2} - \bar{y}\sin\theta\right) & 0 & 0 \\ 0 & 0 & f(p,d,t_{\mathrm{TF}},t_{\mathrm{BF}},t_w,\theta) & 0 & 0 & 0 \\ 0 & 0 & 0 & -\cos\theta & 0 & 0 \\ 0 & 0 & 0 & 0 & g(p,d,t_{\mathrm{TF}},t_{\mathrm{BF}},t_w,\theta) & 0 \\ 0 & 0 & 0 & 0 & 0 & 1 \end{bmatrix} \begin{Bmatrix} \varepsilon_{xo} \\ \varepsilon_{yo} \\ \gamma_{xyo} \\ \kappa_x \\ \kappa_y \\ \kappa_{xy} \end{Bmatrix}^{(M)} \tag{19}$$

The refined transformation matrix contains a Poisson's ratio that takes into account the lateral contraction or elongation $\varepsilon_{\bar{y}o}$ of the web due to a unit macromidplane strain in the x direction $\varepsilon_{\bar{x}o}$ and a unit macrocurvature in the x direction κ_x. The micromidplane strains $\varepsilon_{\bar{y}o}$, $\gamma_{\overline{xy}o}$ in the web due to either $\kappa_y^M = 1$ or $\kappa_{xy}^M = 1$ were removed because there is no force in the $\bar{y}$ direction that is causing a midplane strain in that direction. From Eq. (9), the relation between macromidplane shear strain and macrocurvature can be given as

$$\gamma_{\overline{xy}o}^{(3)} = \gamma_{xy}^M \cos\theta \tag{20}$$

$$\kappa_{\bar{y}}^{(3)} = \kappa_x^M (\cos^3\theta + 2\cos\theta \sin^2\theta) \tag{21}$$

Equations (20) and (21) treat the web as an unresisting member of the unit cell when it is deforming. For example, when the unit cell undergoes a unit midplane shear strain or a unit curvature, the faces are compliant with that deformation but the webs resist that movement. Equations (20) and (21) will be true if the webs were at a right angle to the face sheet. The equations were proved wrong in general and our assumption that the webs resist deformation was proved right by conducting several finite element analyses for various web angle inclinations. An analytical procedure that takes into account the webs resistance to deformation was established to determine the micromidplane shear strain and microcurvature, i.e., $f(p,d,t_{\mathrm{TF}},t_{\mathrm{BF}},t_w,\theta)$, $g(p,d,t_{\mathrm{TF}},t_{\mathrm{BF}},t_w,\theta)$.

1. *Micromidplane Shear Strain in the Webs*

An analytical procedure was determined that relates macromidplane shear strain to micromidplane shear strain. The analytical method takes into account the resistance to shear that the webs will experience when the unit cell is under midplane shear. The top and bottom face sheets were investigated separately under the action of shear (Fig. 5). It can be seen from Fig. 5 that we are including the resistance to shear by the webs through a shear force acting on the webs F_w.

The total top face, bottom face, and web shear strain are as follows.

$$\gamma^{(1)} = \frac{1}{p}[\gamma_1 f + \gamma_2 (p - f)] \tag{22}$$

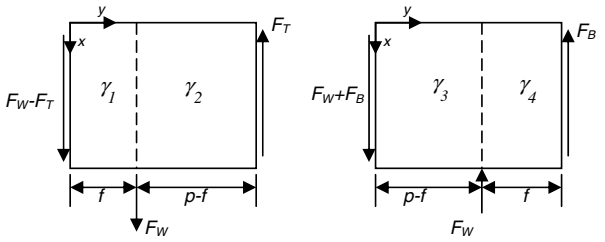

a) Top face sheet **b) Bottom face sheet**

Fig. 5 Free body diagram of the face sheet under the action of midplane shear strain.

$$\gamma^{(2)} = \frac{1}{p}[\gamma_4 f + \gamma_3(p-f)] \tag{23}$$

$$\gamma^{(3)} = \frac{1}{s}[\gamma_1 f - \gamma_3(p-f)] \tag{24}$$

The shear strain in the faces and webs due to the shearing forces are defined as follows.

$$\gamma_1 = \frac{F_W - F_T}{t_{\mathrm{TF}} G_{\mathrm{TF}}} \qquad \gamma_2 = \frac{-F_T}{t_{\mathrm{TF}} G_{\mathrm{TF}}} \qquad \gamma_3 = \frac{F_W + F_B}{t_{\mathrm{BF}} G_{\mathrm{BF}}} \qquad \gamma_4 = \frac{-F_B}{t_{\mathrm{BF}} G_{\mathrm{BF}}} \tag{25}$$

The shear force in the webs is

$$F_w = G_w t_w \gamma_w \tag{26}$$

There are three unknown shear forces F_T, F_w, F_B. The three unknown forces were determined by solving a system of three linear equations with the three unknowns, shown as follows:

$$\gamma^{(1)} = 1 \qquad \gamma^{(2)} = 1 \qquad 0 = G_w t_w \gamma_w - F_w \tag{27}$$

Solving Eq. (27) yields the three shear forces that act on the faces during shear. Substituting the known shear forces from Eq. (27) into the web shear strain equation in Eq. (24) yields the macro- to micromidplane shear strain relation of the web.

$$f(p, d, t_{\mathrm{TF}}, t_{\mathrm{BF}}, t_w, \theta) = \gamma^{(3)} = \frac{1}{s}[\gamma_1 f - \gamma_3(p-f)] \tag{28}$$

2. Microcurvature in the $\bar{y}$ Direction for the Webs

An analytical procedure is derived that relates macro-y-direction curvature to micro-$\bar{y}$-direction curvature in the webs. The analytical method takes into account the resistance to curvature that the webs will experience when the unit cell is under the y-direction curvature. Half of the unit cell was investigated under the action of couples that act on the faces (Fig. 6).

Consider the half-unit cell under the action of an end couple that will cause unit curvature in the y direction. The half-unit-cell end couple was represented as three end couples acting on the faces and webs (C_T, C_w, and C_B). The slopes of the faces and web due to an end couple were obtained from beam theory (one-dimensional plate) formulas [17]. There are three unknown constants (C_T, C_w, and C_B) in Fig. 6. To solve the three unknowns we need a system of three linear equations. The three equations come from the boundary conditions. The first two boundary conditions are that the slopes of the top and bottom face sheet must equal the slopes of the faces when $\kappa_y^M = 1$. The last boundary condition is that the difference of slope between the face and web junction point (A and B) must equal the slope of the web. After solving the system of linear equations, the curvature of the webs was determined by dividing the couple acting on the web by the flexural stiffness of the web (equivalent EI).

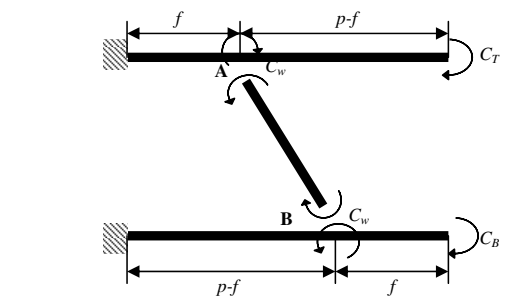

Fig. 6 Half-unit-cell under the action of end couples at the faces.

$$\frac{(C_T + C_w)f}{(EI)_{\mathrm{TF}}} + \frac{C_T(p-f)}{(EI)_{\mathrm{TF}}} = p \tag{29}$$

$$\frac{(C_B - C_w)(p-f)}{(EI)_{\mathrm{BF}}} + \frac{C_B f}{(EI)_{\mathrm{BF}}} = p \tag{30}$$

$$\frac{(C_B - C_w)(p-f)}{(EI)_{\mathrm{BF}}} - \frac{(C_B + C_w)f}{(EI)_{\mathrm{TF}}} = \frac{C_w s}{(EI)_w} \tag{31}$$

$$g(p, d, t_{\mathrm{TF}}, t_{\mathrm{BF}}, t_w, \theta) = \kappa_{\bar{y}}^{(3)} = \frac{C_w}{(EI)_w} \tag{32}$$

F. Formulation of Transverse Shear Stiffness A_{55}

For a corrugated-core sandwich structure loaded in shear transverse to the corrugations (by shear stress τ_{xz} or shear force Q_x), it is recognized that the face sheets and core will undergo bending deformation [7,18]. For the determination of A_{55}, the shear stress in the face sheets are neglected because of its small thickness and classical plate theory is used. To determine the shearing stiffness due to Q_x, we must first identify the shear stresses in the webs due to Q_x. Figure 7 shows a free body diagram of the corrugated-core panel unit of length dx in the x direction where only the stresses which act in the x direction are shown and considered. The stress values shown are average stresses over the faces of an element which is assumed to be very small. A summation of the forces in the x direction yields

$$\left(F + \frac{\partial F}{\partial x}\Delta x - F\right)\Delta y \Delta z + 2\left[\tau_{zx}\Delta x\left(\frac{t_c s}{d}\right)\right]\Delta y \Delta z = 0 \tag{33}$$

Following the procedure in Appendix B, we determined the shear stresses in the webs $\tau_{\overline{xy}}$ due to Q_x. The shear strain-energy density (strain energy per unit area of the sandwich panel) can be calculated either from the web shear stresses given in Eq. (B6), Appendix B, or from the shear force Q_x and yet to be determined shear stiffness A_{55}. By equating the two shear strain-energy density terms we obtain

$$U_s = \frac{t_c}{p}\int_0^s \frac{1}{2}\frac{(\tau_{\overline{xy}})^2}{G_{\overline{xy}}}\,\mathrm{d}\bar{y} = \frac{Q_x^2}{2A_{55}} \tag{34}$$

Using Eq. (34), the equivalent shear stiffness A_{55} of the sandwich panel was solved.

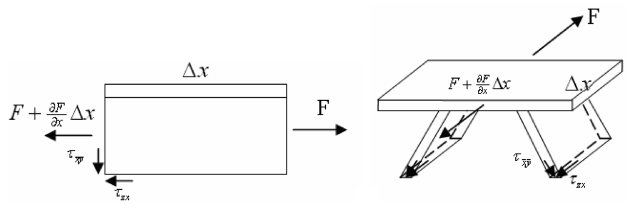

a) **b)**

Fig. 7 Small element removed from a body, showing the stresses acting in the x direction only: a) side view, b) isometric view.

G. Formulation of the Transverse Shear Stiffness A_{44}

Formulation of the transverse shear stiffness A_{44} of the panel is relatively complicated [11] because certain conditions need to be fulfilled. Figure 8a shows a sandwich panel of unit length in the x direction subjected to unit transverse shear $Q_y = 1$. The horizontal force $Y = p/d$ provides equilibrium.

Point A in Fig. 8b is assumed to be fixed to eliminate rigid body movements of the unit cell. The relative displacements δ_y and δ_z will result from the transverse shearing and horizontal force. Because the force is small, the displacements will be proportional to Q_y, thus an average shear strain is represented as

$$\gamma_y = \frac{\delta_y}{d} + \frac{\delta_z}{p} \tag{35}$$

Because of antisymmetry, only half of the unit cell needs to be considered for analysis (Fig. 9a). The unit shear force resultant is divided into a force P acting on the top face sheet and a force R acting on the lower face sheet. A shear force F is assumed to act on the top face sheet at point A where there are no horizontal forces due to antisymmetry, and a force (1-F) was determined through a summation of the forces in the z direction. The displacements of the half-unit cell under the action of force P, R, and F is shown in Fig. 9b.

From Figs. 9a and 9b we observed that there are three unknown forces and five displacements that need to be solved. These forces and displacements can be solved through the energy method. The total strain energy in half the unit cell is the sum of the strain energies from each individual member (i.e., AB, BC, DE, BE, EG). The strain energy due to a bending moment is considered, whereas the strain energy due to shear and normal forces are neglected. The total strain energy in Fig. 9a is shown in Appendix C.

Using Castigliano's theorem, Eq. (36), which states that displacement is equal to the first partial derivative of the strain energy in the body with respect to the force acting at the point and in the direction of displacement [19], the unknown forces and displacements can be determined.

$$\delta_i = \frac{\partial U_i}{\partial P_i} \tag{36}$$

Because the overall thickness of the sandwich panel remains constant during distortion, the boundary conditions are $\delta_z^C = \delta_z^G$ and $\delta_z^A = 0$. Because half the unit cell is under unit shear then $P + R = 1$. The two boundary conditions along with Castigiliano's second theorem lead to a system of two linear equations with two unknowns.

$$\frac{\partial U_s}{\partial F} = 0 \tag{37}$$

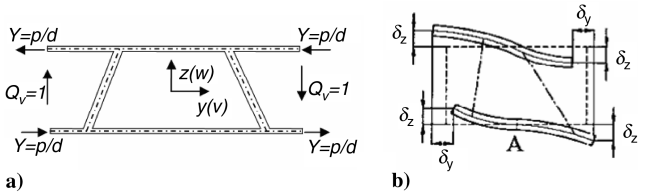

Fig. 8 Unit transverse shear and horizontal force: a) unit cell, b) deformations [8].

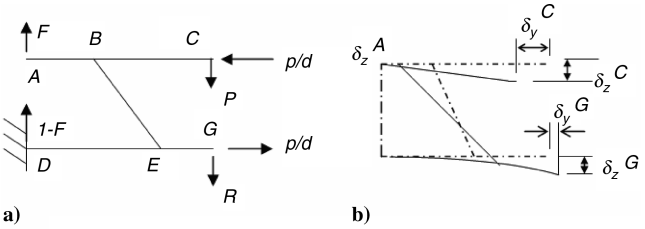

Fig. 9 Half-unit-cell a) corrugated-core sandwich panel, b) deformations.

$$\frac{\partial U_s}{\partial P} = \frac{\partial U_s}{\partial R} \tag{38}$$

The unknown forces P, F, R were determined by substituting Eq. (C1) from Appendix C into Eqs. (37) and (38) and solving the system of linear equations. The expressions for the forces P, F, and R are quite lengthy, and so they are omitted in this paper. The half-unit-cell displacements were determined by using Eq. (C1) from Appendix C and Eq. (36) along with the values of the unknown forces (refer to Appendix C). The displacement of the half-unit cell are $\delta_y = \delta_y^C + \delta_y^G$ and $\delta_z = \delta_z^C = \delta_z^G$ in the y and z directions. Using the force-distortion relationships developed by Libove and Batdorf [12] to describe the elastic behavior of an orthotropic thick plate, the transverse shear stiffness A_{44} was obtained as follows:

$$A_{44} = \frac{Q_y}{\gamma_y} = \frac{1}{\delta_y/d + \delta_z/p} = \frac{1}{(1/d)\left(\delta_y^C + \delta_y^G\right) + (1/p)\delta_z^C} \tag{39}$$

IV. Response of the ITPS Panel as a Two-Dimensional Plate

An ITPS panel forms the outer skin of the vehicle, which covers the crew compartment. The ITPS panel experiences thermal forces and moments due to the extreme reentry temperatures as well as a pressure load which comes from the pressurized crew compartment or from the transverse aerodynamic pressure. All those conditions could cause the panel to deflect, buckle, and yield. Knowing the panel deflection and failure modes is important because excessive deflection of the panel can lead to extremely high local aerodynamic heating. Local buckling can be a major design driver because the panel is composed of thin plates. A two-dimensional plate analysis is needed to determine the behavior of the ITPS when it is subjected to those various loading conditions. Consider a simply supported orthotropic sandwich panel of width b (y direction) and length a (x direction) as illustrated in Fig. 3, the boundary conditions may be described as

$$\begin{aligned} &w(0,y) = 0, \quad w(a,y) = 0 \quad M_x(0,y) = 0, \quad M_x(a,y) = 0 \\ &w(x,0) = 0, \quad w(x,b) = 0 \quad M_x(x,0) = 0, \quad M_x(x,b) = 0 \end{aligned} \tag{40}$$

The panel is subject to a pressure load

$$P_Z = -\sum_{m=1}^{\infty}\sum_{n=1}^{\infty} P_{mn} \sin\left(\frac{m\pi x}{a}\right) \sin\left(\frac{n\pi y}{b}\right) \tag{41}$$

where $P_{mn} = (16P_o)/(\pi^2 mn)$ and P_o is the uniform load. The panel is also assumed to have the following deformations:

$$w(x,y) = \sum_{m=1}^{\infty}\sum_{n=1}^{\infty} A_{mn} \sin\left(\frac{m\pi x}{a}\right) \sin\left(\frac{n\pi y}{b}\right) \tag{42a}$$

$$\psi_x(x,y) = \sum_{m=1}^{\infty}\sum_{n=1}^{\infty} B_{mn} \cos\left(\frac{m\pi x}{a}\right) \sin\left(\frac{n\pi y}{b}\right) \tag{42b}$$

$$\psi_y(x,y) = \sum_{m=1}^{\infty}\sum_{n=1}^{\infty} C_{mn} \sin\left(\frac{m\pi x}{a}\right) \cos\left(\frac{n\pi y}{b}\right) \tag{42c}$$

In Eq. (42), $w(x,y)$ is the out-of-plane displacement, and $\psi_x(x,y)$ and $\psi_y(x,y)$ are the plate rotations. Using the FSDT, the effect of shear deformation on deflections and stresses can be investigated. The unknown constants A_{mn}, B_{mn}, C_{mn} are obtained by substituting the constitutive relations in the form of the assumed deformations into the differential equation of equilibrium. Doing so will yield a

system of three linear equations and three unknowns (refer to Appendix D). Solving for the unknown constants, one can now determine the deflections at a given x and y coordinate on the two-dimensional orthotropic sandwich panel. The results in the series converged for $m = n = 23$ [8].

V. Results

A. Extensional and Bending Stiffness

For verification of the effectiveness of the analytical models, consider an ITPS sandwich panel with the following dimensions: $p = 80$ mm, $d = 80$ mm, $t_{\mathrm{TF}} = 1$ mm, $t_{\mathrm{BF}} = 1$ mm, $t_w = 1$ mm, $\theta = 75$ deg, $a = 0.65$ m, $b = 0.65$ m. An AS/3501 graphite/epoxy composite, $E_1 = 138$ GPa, $E_2 = 9$ GPa, $\upsilon_{12} = 0.3$, $G_{12} = 6.9$ GPa, with four laminae in each component and a stacking sequence of $[(0/90)_2]$ was used as an example to verify the analytical models. A finite element analysis was conducted on the unit cell using the commercial ABAQUS finite element program (see Fig. 10). Eight-node shell elements were used to model the face sheets and webs of the unit cell. The shell elements have the capability to include multiple layers of different material properties and thicknesses. Three integration points were used through the thickness of the shell elements. The FEM model consisted of 18,240 nodes and 6000 elements.

The ITPS plate stiffness was obtained by modeling the unit cell with shell elements and subjecting the unit cell to six linearly independent deformations. The six linearly independent strains are 1) $\varepsilon^M_{xo} = 1$ and maintaining the rest of the macroscopic strains and curvature zero; 2) $\varepsilon^M_{yo} = 1$ and maintaining the remaining strains and curvature zero; and, similarly, 3) $\gamma^M_{xyo} = 1$; 4) $\kappa^M_x = 1$; 5) $\kappa^M_y = 1$; and 6) $\kappa^M_{xy} = 1$. Strains were imposed by enforcing periodic displacement boundary conditions on the unit cell (Table 1). To prevent rigid body motion and translation, the unit cell (Fig. 11) was subjected to minimum support constraints. The top and bottom surfaces were assumed to be free of traction. The faces $x = 0$ and $x = a$ have identical nodes on each side as well as the other faces $y = 0$ and $y = b$. The identical nodes on the opposite faces are constrained to enforce the periodic boundary conditions. Figure 12 shows the deformations of the unit cell as a result of imposing the periodic boundary conditions.

The nodal forces of the boundary nodes were obtained from the finite element output after the analyses. Nodal moments were obtained by multiplying the nodal forces with the distance from the midplane. These nodal forces and moments of the boundary nodes were then summed to obtain the force and moment resultants, Eq. (43). The stiffness coefficients in the column corresponding to the nonzero deformation were computed by substituting the values from Eq. (43) into the plate constitutive relation. The same procedure was repeated for other deformation components to obtain and fully populate the unit-cell stiffness coefficients.

$$[N_i, M_i] = \left(\frac{1}{b}\right) \sum_{m=1}^{n} [1, z] F_i^{(m)}(a, y, z) \tag{43}$$

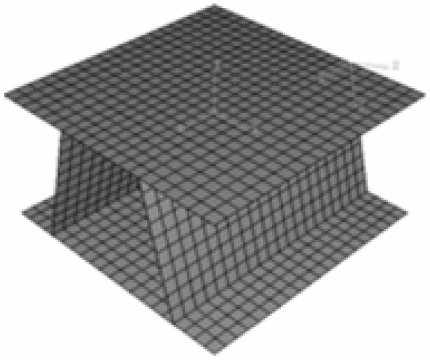

Fig. 10 Finite element mesh of the unit cell.

Table 1 Periodic displacement boundary conditions imposed on the lateral faces of unit cell

	$u(a,y)-u(0,y)$	$v(a,y)-v(0,y)$	$w(a,y)-w(0,y)$	$u(x,b)-u(x,0)$	$v(x,b)-v(x,0)$	$w(x,b)-w(x,0)$	$\theta_x(a,y)-\theta_x(0,y)$	$\theta_y(a,y)-\theta_y(0,y)$	$\theta_x(x,b)-\theta_x(x,0)$	$\theta_y(x,b)-\theta_y(x,0)$
$\varepsilon_{x0} = 1$	a	0	0	0	0	0	0	0	0	0
$\varepsilon_{y0} = 1$	0	0	0	0	b	0	0	0	0	0
$\gamma_{xy0} = 1$	0	$a/2$	0	$b/2$	0	0	0	0	0	0
$\kappa_x = 1$	az	0	$-a^2/2$	0	0	0	0	a	0	0
$\kappa_y = 1$	0	0	0	0	bz	$-b^2/2$	0	0	$-b$	0
$\kappa_{xy} = 1$	0	$az/2$	$-ay/2$	$bz/2$	0	$-bx/2$	$-a/2$	0	0	$b/2$

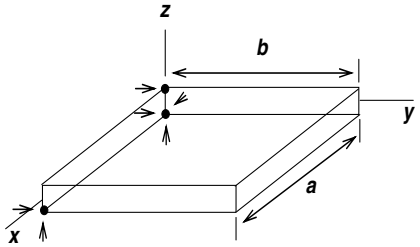

Fig. 11 Boundary conditions imposed on the plate to prevent rigid body motion. An arrow pointing at a black dot indicates displacement of that point is fixed in the direction of the arrow.

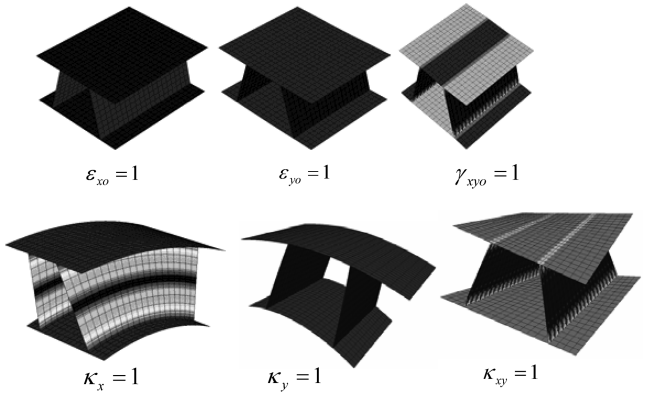

Fig. 12 Deformations of the unit cell due to imposed periodic boundary conditions.

The finite element result from Table 2 indicates that using Eq. (15) provides an excellent prediction to determine the extensional, coupling, and bending stiffness of an ITPS panel. The finite element results have a less than 2% difference in agreement with the analytical results obtained from the strain-energy method.

B. Stress Verification

1. *Midplane Shear Strain and Curvature in the Webs*

Consider the same FEM unit-cell representative volume element and mesh from Fig. 10 with the same material properties and cross-ply lay-up. The web angle inclination was changed from 55 to 90 deg and the unit cell was subjected to a periodic unit midplane shear strain and a periodic *y*-direction curvature separately. The corresponding web midplane shear strain and web curvature were extracted from the FEM output after analysis. The results of midplane shear strain and curvature from FEM and Eqs. (28) and (32) are compared in Fig. 13.

From Fig. 13, one can note that there is a less than 2% difference between the FEM and analytical results of Eqs. (28) and (32). The analytical equations do an excellent job in accounting for the resistance effect of the webs when the unit cell is subjected to a midplane shear or bending in the macroscale sense. This gives us the confidence that we will obtain accurate stress results when compared with the FEM.

2. *Stress Verification*

The refined web stress deformation transformation matrix was verified by a finite element analysis. A known strain was applied to the unit cell and the corresponding stresses on the faces and webs were obtained from Eq. (17). The known strain was applied to the finite element model by enforcing periodic displacement boundary conditions from Table 1. The stress results from the FEM output after analysis and Eq. (17) were plotted in Figs. 14–19. In Figs. 14–19, all values in the *y* axis are normalized with respect to either the face thickness or web length. In these figures, TF and BF stand for top face and bottom face, respectively, F is the finite element, A stands for analytical, and where included, 0 and 90 deg indicate lamina orientation.

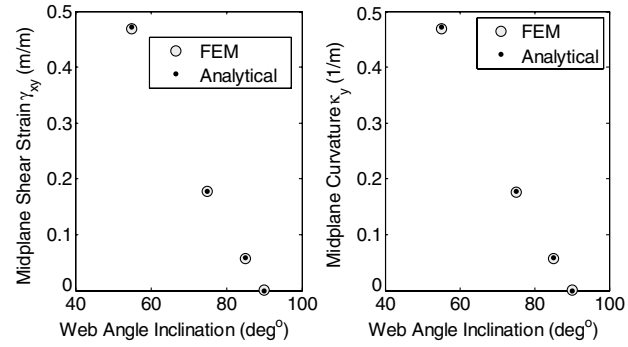

Fig. 13 Comparison of FEM and analytical midplane shear strain/curvature in the web for a given shear strain/curvature of the unit cell.

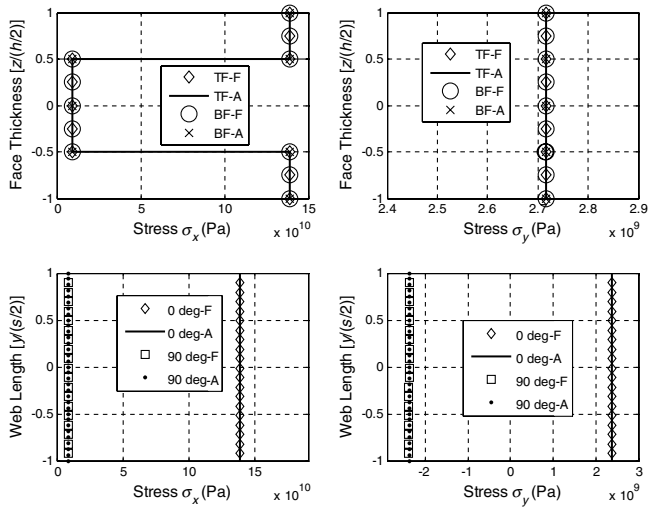

Fig. 14 Stresses in the *x* and *y* direction in the top face, bottom face, and web for a unit-cell strain of $\varepsilon_{xo}^{M} = 1$.

The analytical results are in excellent agreement with the finite element output. Results from the FEM stress output validate the procedure of the derived stress equations of an ITPS sandwich panel. All stress results in Figs. 14–19 have less than a 4% difference from the FEM results. The refined web stress deformation transformation matrix does an excellent job in predicting strain in the webs which results in stress data that are in good agreement with the FEM output. Furthermore, the refined web stress deformation transformation matrix does not alter the stiffness matrix. The refined web stress deformation transformation matrices from Eq. (15) were used to compute the ITPS stiffness as shown in Table 3. Analytical-1 includes the stiffness results obtained from using the deformation transformation matrices from Eqs. (5), (6), (8), and (9). Analytical-2 includes the stiffness results obtained from using the deformation transformation matrices from Eqs. (5) and (6) and the refined web

Table 2 Nonzero [*A*], [*B*], and [*D*] coefficients for an ITPS sandwich panel

Stiffness	A_{11}, N/m	A_{12}, N/m	A_{22}, N/m	A_{66}, N/m	D_{11}, N · m	D_{12}, N · m	D_{22}, N · m	D_{66}, N · m
Analytical	2.23E + 08	5.43E + 06	1.48E + 08	1.43E + 07	2.76E + 05	8790	2.37E + 05	22,327
FE	2.20E + 08	5.43E + 06	1.48E + 08	1.41E + 07	2.78E + 05	8690	2.37E + 05	22,200
% difference	1.35	0	0	0.89	0.63	1.09	0.13	0.6

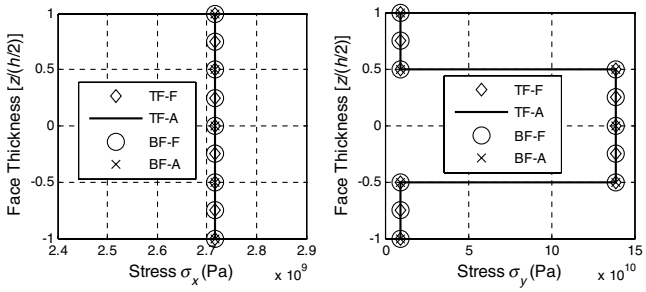

Fig. 15 Stresses in the x and y direction in the top face and bottom face for a unit-cell strain of $\varepsilon_{yo}^{M} = 1$.

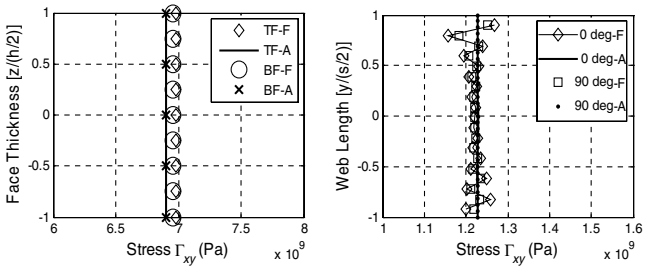

Fig. 16 Shear stresses in the top face, bottom face, and web for a unit-cell strain of $\gamma_{xyo}^{M} = 1$.

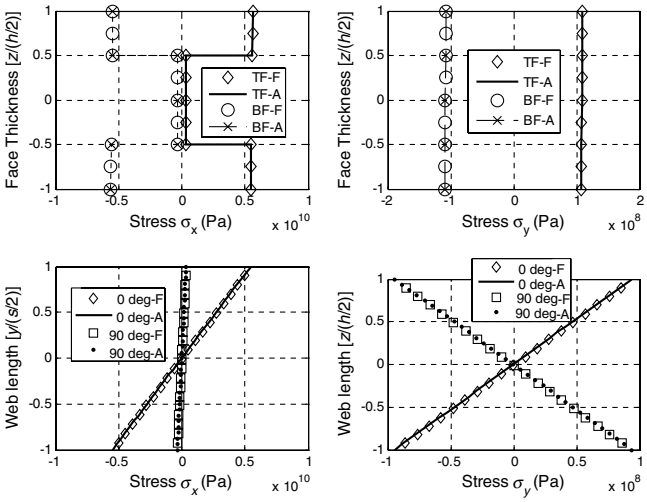

Fig. 17 Stresses in the x and y direction in the top face, bottom face, and web for a unit-cell strain of $\kappa_x^{M} = 1$.

stress deformation transformation matrices from Eqs. (18) and (19). The refined web stress deformation transformation matrices have the capability to accurately predict stresses in each unit-cell component and accurately predict the ITPS stiffness. The previously derived deformation transformation matrices outputs excellent stiffness results but erroneous stress results. The refined web stress deformation transformation matrices outputs excellent stiffness results and accurate stress results when compared with finite element analysis.

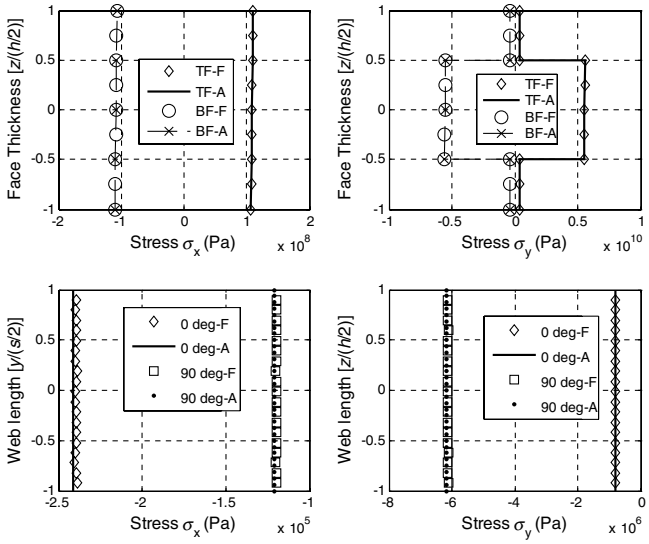

Fig. 18 Stresses in the x and y direction in the top face, bottom face, and web for a unit-cell strain of $\kappa_y^{M} = 1$.

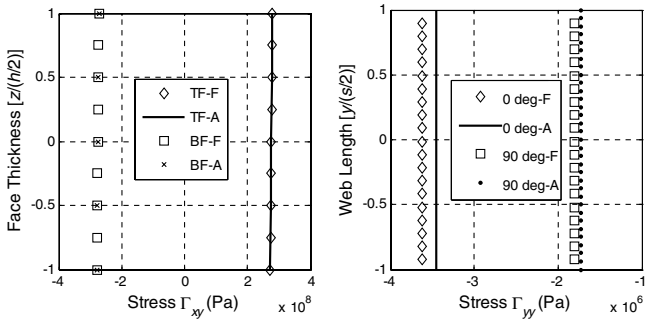

Fig. 19 Shear stresses in the top face, bottom face, and web for a unit-cell strain of $\kappa_{xy}^{M} = 1$.

C. Transverse Shear Stiffness Verification

The finite element verification of the A_{44} stiffness term consisted of a two-part finite element procedure. First, we assumed that the unit cell behaves like a cantilevered one-dimensional plate and determined the equivalent cross-sectional properties from finite element analysis. The equivalent cross-sectional properties are axial rigidity EA, flexural rigidity EI, and shear rigidity A_{44}. The beam consisted of 10 ITPS unit cells and was clamped on the left end, Fig. 20. Eight-node solid elements were used to model the one-dimensional plate. First an end couple was applied and the corresponding tip deflections were determined from the finite element output after analyses. The tip deflection can also be derived as

$$v_{\text{tip}} = \frac{Ml^2}{2EI} \tag{44}$$

Using Eq. (44), we determined the flexural rigidity EI. The couple was then removed and a transverse force was applied at the tip. The tip deflections were obtained from the finite element output. Again the tip deflection is given by

Table 3 Nonzero [A], [B], and [D] coefficients for an ITPS sandwich panel

Stiffness	A_{11}, N/m	A_{12}, N/m	A_{22}, N/m	A_{66}, N/m	D_{11}, N · m	D_{12}, N · m	D_{22}, N · m	D_{66}, N · m
Analytical-1	2.235E + 08	5.432E + 06	1.479E + 08	1.427E + 07	275,920	8788.2	236,770	22,327
Analytical-2	2.234E + 08	5.432E + 06	1.479E + 08	1.402E + 07	275,870	8691.5	236,590	22,082
FE	2.204E + 08	5.432E + 06	1.479E + 08	1.414E + 07	277,640	8691	236,590	22,100
% diff. (FE-1)	1.37%	0.00%	0.00%	0.98%	0.62%	1.12%	0.08%	1.03%
% diff. (FE-2)	1.33%	0.00%	0.00%	0.79%	0.64%	0.01%	0.00%	0.08%

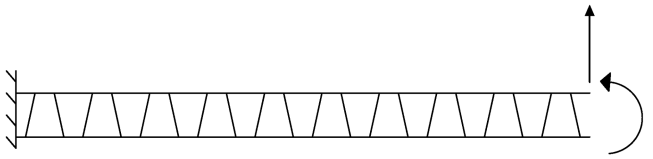

Fig. 20 Corrugated-core modeled as a cantilever beam with ten unit cells.

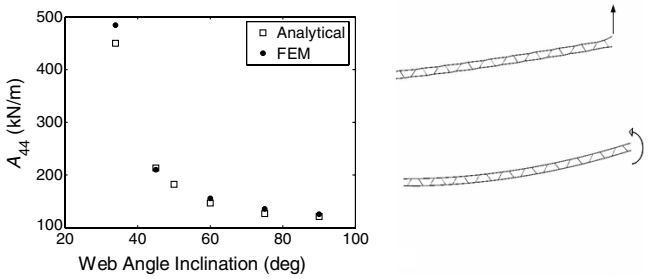

Fig. 21 Transverse shearing stiffness a) finite element and analytical results, b) deformation of the corrugated-core sandwich panel as a beam.

$$v_{\text{tip}} = \frac{Fl^3}{3EI} + \frac{Fl}{A_{44}} \tag{45}$$

Using finite element tip deflection in Eq. (45) along with the flexural rigidity result from Eq. (44) we determined the shear rigidity A_{44}. This finite element verification procedure was done for various web angles. The finite element result along with the analytical result from Eq. (39) is shown in Fig. 21. The finite element results are in good agreement with the analytical formulation of A_{44}. The percentage difference between the finite element results and the analytical result does not exceed 7%. The finite element deformation of the cantilever beam is shown in Fig. 21b.

D. Two-Dimensional Orthotropic Plate Results

To determine the optimal web angle inclination for greatest stiffness and minimum center panel deflection, we investigated the variation of the stiffness and center panel deflection to a change of web angle of inclination. Changes in A_{44} are important because certain applications depend on the behavior in this plane. Maximum panel deflection is important because excessive deflection of the ITPS panel can lead to high local aerodynamic heating. Consider an ITPS sandwich panel with the following dimensions: $p = 80$ mm, $d = 80$ mm, $t_{\text{TF}} = 1$ mm, $t_{\text{BF}} = 1$ mm, $t_w = 1$ mm, $a = 0.64$ m, $b = 0.64$ m; such a panel is composed of four unit cells. The sandwich panel is made out of graphite/epoxy T300/934: $E_1 = 138$ GPa, $E_2 = 9$ GPa, $G_{12} = 6.9$ GPa, $\upsilon_{12} = 0.3$, with four laminae in each component and a stacking sequence of $[0/90]_s$. By prescribing an internal web angle, the thickness of the faces and webs is defined such that the ITPS sandwich's cross-sectional area (thus the weight) remains the same to the 90 deg web angle configuration. Doing so will allow us to only get the behavior of stiffness to a change in angle rather than a change in angle and area. The results are shown in Figs. 22 and 23. The closed-form solution deflection results of the ITPS plate are compared with the ABAQUS finite element program. Because of the symmetry of the uniform loading and boundary conditions, only a quarter of the panel was used in the model. The FE model consisted of eight-node shell elements.

From Fig. 23, the following conclusions can be made:

1) The highest bending, extensional, and transverse shear stiffness A_{55} are provided by the corrugated-core panel with vertical webs.

2) Whereas the bending, extensional, and A_{55} shear stiffness decreases with decreasing web angle inclination, the transverse shear stiffness A_{44} increases.

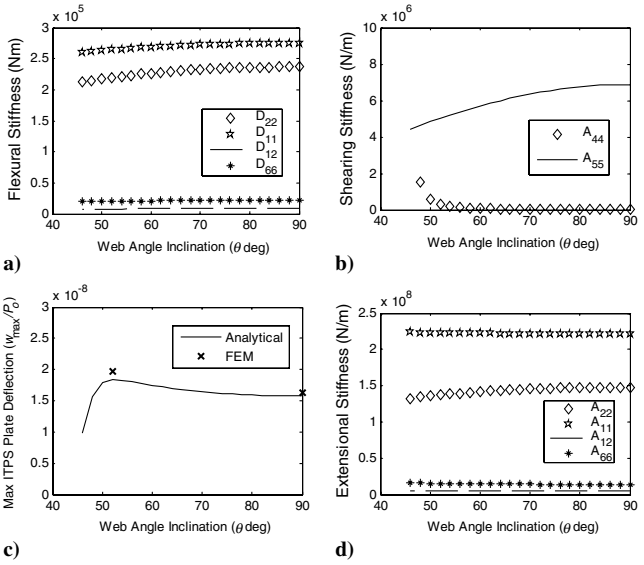

Fig. 22 Behavior of a) D-matrix, b) shear stiffness, c) maximum deflection, and d) bending stiffness, as a function of web inclination angle.

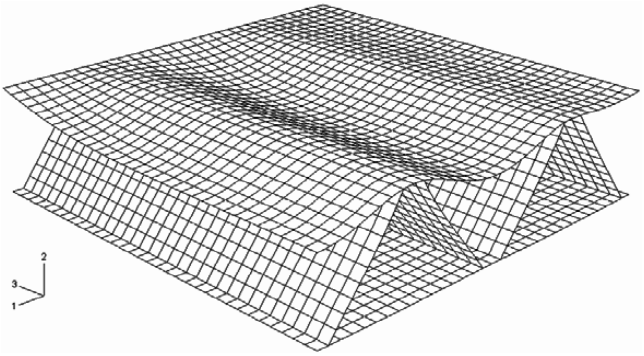

Fig. 23 Exaggerated deformed mesh (deformation scale factor = 2).

3) Maximum deflection occurred at the 52 deg web angle inclination, and minimum deflection occurred at the triangular web configuration.

4) A_{44} is the most dominant stiffness when the corrugated-core sandwich panel has triangular webs.

5) For panels with rectangular web configurations, its behavior is dominated by shear deformation in the y direction.

6) Maximum deflections computed from the closed-form solution agree very well with the finite element results. The percentage difference between the FEM results and the analytical results at 52 and 90 deg web angle inclination is 6.17 and 3.15%, respectively. An accurate prediction when compared with the FEM of the shearing term is made for rectangular web configurations which lead to accurate deflection results.

In design, a triangular corrugated core may be preferred because the influence on shear can be neglected due to the high stiffness, and the maximum plate deflection is at a minimum. By neglecting shear effects, the plate response can be analyzed by classical laminate plate theory (CLPT). However, that type of configuration poses problems such as local buckling because of the long unsupported lengths of the webs.

VI. Conclusions

Finite element analysis is commonly used to analyze sandwich structures. However, a full three-dimensional finite element analysis is not economical for a preliminary analysis of a structure. Such panels can be represented as an orthotropic thick plate for which analytical solutions can be derived. A method to homogenize the

corrugated sandwich panel into an orthotropic thick plate has been presented. Detailed formulation of the bending, extensional, coupling, and shear stiffness for the unit corrugated-core sandwich panel was presented and verified. Panels with rectangular webs resulted in a weak extensional, bending, and A_{55} stiffness. The analytical models are capable of handling laminated composite materials for the face sheets and webs of the sandwich panel. Furthermore, one can use different materials for the face sheets and web. For example, the hot side (outer) face sheet can use ceramic matrix composite and the cool side (inner) face sheet can use polymer matrix composites. The webs can be composed of other materials such as titanium, aluminum, or composite. The stiffness results between the analytical model and the finite element analysis were within 2%, thus validating the method presented in this study. The refined web stress deformation transformation matrix made incremental improvements to the ITPS stiffness when compared with FE results. Both the deformation transformation matrix for the webs and the refined web stress deformation transformation matrix can be used in determining ITPS stiffness, but only the latter matrix can be used for stiffness and stress prediction. The computational time and effort in determining stiffness and plate behavior of the ITPS were significantly reduced in comparison with FEM.

The equivalent stiffness parameters were used in the closed-form solution to evaluate the maximum deflection of the sandwich panel when subjected to a uniform pressure load. Maximum deflection was greatest for 52 deg web configuration for the example considered. Maximum deflection was fairly constant for the web angle range of 80–90 deg. Panels with triangular web configuration have negligible shear deformation effect because of the high shearing stiffness in both directions, but this leads to other problems such as local buckling. Global buckling of the panel is not expected because the ITPS panel is expected to be thick. However, local buckling is a factor because the face sheets and the webs are made of thin plates. A triangular web configuration will result in the web length to be long as well as the length between the adjoining unit cell. The increased length will lead to a lower critical buckling value. A high critical buckling value is desirable to avoid local buckling of the ITPS panel.

Appendix A: Right Web Transformation Matrix Determination

The rotation and translation matrix that relates the local and global axes of the ITPS unit cell is shown.

$$\begin{Bmatrix} x \\ y \\ z \end{Bmatrix} = \begin{bmatrix} 1 & 0 & 0 \\ 0 & \cos\theta & \sin\theta \\ 0 & -\sin\theta & \cos\theta \end{bmatrix} \begin{Bmatrix} \bar{x} \\ \bar{y} \\ \bar{z} \end{Bmatrix} + \begin{Bmatrix} 0 \\ f \\ \frac{d_c}{2} \end{Bmatrix} \tag{A1}$$

$$\begin{Bmatrix} \bar{u} \\ \bar{v} \\ \bar{w} \end{Bmatrix} = \begin{bmatrix} 1 & 0 & 0 \\ 0 & \cos\theta & -\sin\theta \\ 0 & \sin\theta & \cos\theta \end{bmatrix} \begin{Bmatrix} u \\ v \\ w \end{Bmatrix} \tag{A2}$$

A detailed procedure of analysis is presented in this section for the derivation of the deformation transformation matrices of the left and right web. Integrating Eq. (7) twice with respect to y results in the out-of-place displacement:

$$w(y) = \frac{1}{2}\kappa_o y^2 \tag{A3}$$

From classical lamination theory, the u and v displacements of the sandwich panel in the global coordinates are determined as shown below:

$$u(x, y, z) = u_o(x, y) - z\frac{\partial w}{\partial x} = 0 \tag{A4a}$$

$$v(x, y, z) = v_o(x, y) - z\frac{\partial w}{\partial y} = \kappa_o yz \tag{A4b}$$

To determine the strains in the web, the displacements from Eq. (A2) must be in the local coordinate system. Substitution of Eq. (A1) into Eqs. (A3) and (A4), and then Eqs. (A3) and (A4) into Eq. (A2) resulted in $\bar{u}(\bar{x}, \bar{y}, \bar{z})$, $\bar{v}(\bar{x}, \bar{y}, \bar{z})$, $\bar{w}(\bar{x}, \bar{y}, \bar{z})$. Using the small strain and displacement assumption,

$$\varepsilon_{\bar{x}} = \frac{\partial \bar{u}}{\partial \bar{x}} = 0 \quad \varepsilon_{\bar{y}} = \frac{\partial \bar{v}}{\partial \bar{y}} = \kappa_o \cos^2\theta\left(-\bar{y}\sin\theta + z\cos\theta + \frac{d_c}{2}\right) \quad \gamma_{\bar{x}\bar{y}} = \frac{\partial \bar{u}}{\partial \bar{y}} + \frac{\partial \bar{v}}{\partial \bar{x}} = 0 \tag{A5a}$$

$$\kappa_{\bar{x}} = -\frac{\partial^2 \bar{w}}{\partial \bar{x}^2} = 0 \quad \kappa_{\bar{y}} = -\frac{\partial^2 \bar{w}}{\partial \bar{y}^2} = 2\kappa_o \cos\theta \sin^2\theta + \kappa_o \cos^3\theta \quad \kappa_{\bar{x}\bar{y}} = -2\frac{\partial^2 \bar{w}}{\partial \bar{x}\partial \bar{y}} = 0 \tag{A5b}$$

Equations Eq. (A5a) and (A5b) describe the micromidplane strains and curvatures in the right web. From Eq. (A5a) we observed that the midplane strain in the $\bar{y}$ direction is

$$\varepsilon_{\bar{y}o} = -\kappa_o \cos^2\theta\left(\frac{d_c}{2} - \bar{y}\sin\theta\right) \tag{A6}$$

The same procedure applies to unit curvature along the x direction, unit twist k_{xy} and unit shear strain in the xy plane. Shown next are the deformation transformation matrices for the left and right webs.

Left web

$$\{\boldsymbol{D}\}^{(e)} = T_D^e\{\boldsymbol{D}\}^M \qquad \begin{Bmatrix} \varepsilon_{\bar{x}o} \\ \varepsilon_{\bar{y}o} \\ \gamma_{\bar{x}\bar{y}o} \\ \kappa_{\bar{x}} \\ \kappa_{\bar{y}} \\ \kappa_{\bar{x}\bar{y}} \end{Bmatrix}^{(3)} = \begin{bmatrix} 1 & 0 & 0 & \left(\frac{d_c}{2} - \bar{y}\sin\theta\right) & 0 & 0 \\ 0 & 0 & 0 & 0 & \cos^2\theta\left(\frac{d_c}{2} - \bar{y}\sin\theta\right) & 0 \\ 0 & 0 & -\cos\theta & 0 & 0 & \cos\theta\left(\frac{d_c}{2} - \bar{y}\sin\theta\right) \\ 0 & 0 & 0 & -\cos\theta & 0 & 0 \\ 0 & 0 & 0 & 0 & -\cos^3\theta - 2\cos\theta\sin^2\theta & 0 \\ 0 & 0 & 0 & 0 & 0 & 1 \end{bmatrix} \begin{Bmatrix} \varepsilon_{xo} \\ \varepsilon_{yo} \\ \gamma_{xyo} \\ \kappa_x \\ \kappa_y \\ \kappa_{xy} \end{Bmatrix}^{(M)} \tag{A7}$$

Right web

$$\{\boldsymbol{D}\}^{(e)} = T_D^e\{\boldsymbol{D}\}^M \qquad \begin{Bmatrix} \varepsilon_{\bar{x}o} \\ \varepsilon_{\bar{y}o} \\ \gamma_{\overline{xy}o} \\ \kappa_{\bar{x}} \\ \kappa_{\bar{y}} \\ \kappa_{\overline{xy}} \end{Bmatrix}^{(4)} = \begin{bmatrix} 1 & 0 & 0 & \left(\frac{d_c}{2} - \bar{y}\sin\theta\right) & 0 & 0 \\ 0 & 0 & 0 & 0 & \cos^2\theta\left(\frac{d_c}{2} - \bar{y}\sin\theta\right) & 0 \\ 0 & 0 & \cos\theta & 0 & 0 & \cos\theta\left(\frac{d_c}{2} - \bar{y}\sin\theta\right) \\ 0 & 0 & 0 & \cos\theta & 0 & 0 \\ 0 & 0 & 0 & 0 & \cos^3\theta + 2\cos\theta\sin^2\theta & 0 \\ 0 & 0 & 0 & 0 & 0 & 1 \end{bmatrix} \begin{Bmatrix} \varepsilon_{xo} \\ \varepsilon_{yo} \\ \gamma_{xyo} \\ \kappa_x \\ \kappa_y \\ \kappa_{xy} \end{Bmatrix}^{(M)} \tag{A8}$$

Appendix B: Detailed Derivation of A_{55}

Starting with Eq. (33) and dividing through by Δx, Δy, Δz gives

$$2\left[\tau_{zx}\left(\frac{t_c s}{d}\right)\right] = -\frac{\partial F}{\partial x} \tag{B1}$$

Recognizing that the forces in the x direction are a summation of the webs and face sheet forces and that $\tau_{zx} = \tau_{\overline{xy}}\sin\theta$ results in

$$2\left[\tau_{\overline{xy}}\sin\theta\left(\frac{t_c s}{d}\right)\right] = -\frac{\partial}{\partial x}\left[N_{\bar{x}}^{(1)}(2p) + 2\int_0^{\bar{s}} N_{\bar{x}}^{(4)}\,\mathrm{d}\bar{y}\right] \tag{B2}$$

Because the force resultant in the webs is a function of $\bar{y}$ from Eqs. (8) and (9), integration must be done from zero to $\bar{s}$, where $\bar{s}$ is an arbitrary length on the web. Substituting Eq. (2) into Eq. (B2) for N_x we obtain

$$2\left[\tau_{\overline{xy}}\sin\theta\left(\frac{t_c s}{d}\right)\right] = -\frac{\partial}{\partial x}\left[(2p)A_{11}^{(1)}\varepsilon_{xo}^{(1)} + 2\int A_{11}^{(3)}\varepsilon_{xo}^{(3)}\,\mathrm{d}\bar{y}\right] \tag{B3}$$

Substituting Eq. (5) and Eq. (8) for $\varepsilon_{xo}^{(e)}$ into Eq. (B3) and noting that when the unit cell is subjected to pure bending moment per unit length M_x with $M_y = M_{xy} = 0$, the resulting curvature is $\kappa_x = D'_{11}M_x$,

$$2\left[\tau_{\overline{xy}}\sin\theta\left(\frac{t_c s}{d}\right)\right] = -\frac{\partial}{\partial x}\left[(2p)A_{11}^{(1)}\frac{d}{2}D'_{11}M_x + 2D'_{11}M_x\int A_{11}^{(3)}\left(\frac{\mathrm{d}c}{2} - \bar{y}\sin\theta\right)\mathrm{d}\bar{y}\right] \tag{B4}$$

where D'_{11} comes from the inverse relation

$$\begin{Bmatrix} \kappa_x \\ \kappa_y \\ \kappa_{xy} \end{Bmatrix} = \begin{bmatrix} D'_{11} & D'_{12} & D'_{16} \\ D'_{12} & D'_{22} & D'_{26} \\ D'_{16} & D'_{26} & D'_{66} \end{bmatrix} \begin{Bmatrix} M_x \\ M_y \\ M_{xy} \end{Bmatrix} \tag{B5}$$

Distributing out M_x and recognizing $\partial M_x/\partial x = Q_x$, Eq. (B4) was solved for $\tau_{\overline{xy}}$, which is the average shear stress in the webs due to the transverse force resultant Q_x.

$$\tau_{\overline{xy}}(\bar{y}) = -Q_x\left(\frac{d}{2st_c\sin\theta}\right) \times \left[pdA_{11}^{(1)}D'_{11} + 2A_{11}^{(3)}D'_{11}\left(\frac{d_c}{2}\bar{y} - \frac{\bar{y}^2}{2}\sin\theta\right)\right] \tag{B6}$$

Appendix C: Transverse Shear Stiffness

Total strain energy in half the unit cell, Fig. 9a, due to a bending moment is shown.

$$U_s = \frac{1}{2}D_{11}^{\prime(1)}\left[\int_0^f M_{AB}^2(y)\,\mathrm{d}y + \int_0^{p-f} M_{CB}^2(y)\,\mathrm{d}y\right] + \frac{1}{2}D_{11}^{\prime(2)}\left[\int_0^{p-f} M_{DE}^2(y)\,\mathrm{d}y + \int_0^f M_{GE}^2(y)\,\mathrm{d}y\right] + \frac{1}{2}D_{11}^{\prime(3)}\int_0^s M_{BE}^2(\bar{y})\,\mathrm{d}\bar{y} \tag{C1}$$

Displacement equations of half the unit cell due to a unit $\underline{Q}_{\underline{y}}$ gives

$$\delta_y^C = -\frac{1}{3}D_{11}^{\prime 3}\left(F\cos\theta - (1-R)\cos\theta - \frac{p\sin\theta}{d}\right)s^3\sin\theta - \frac{1}{2}D_{11}^{\prime 3}[Ff + (1-R)(p-f)]s^s\sin\theta \tag{C2}$$

$$\delta_y^G = \frac{1}{2}D_{11}^{\prime(2)}d(1-F)(p-f)^2 \tag{C3}$$

$$\delta_z^G = D_{11}^{\prime(2)}\left[(1-F)(p-f)^2\left(\frac{1}{3}(p-f) - \frac{1}{2}p\right) + \frac{1}{3}Rf^3\right] \tag{C4}$$

Appendix D: ITPS Panel as a Two-Dimensional Plate

Constitutive relations and differential equations of equilibrium of the first-order shear-deformable plate theory are as follows.

$$\frac{\partial M_x}{\partial x} + \frac{\partial M_{xy}}{\partial y} - Q_x = 0 \qquad \frac{\partial M_{xy}}{\partial x} + \frac{\partial M_y}{\partial y} - Q_y = 0 \qquad \frac{\partial Q_x}{\partial x} + \frac{\partial Q_y}{\partial y} + P_z = 0 \tag{D1}$$

$$\begin{Bmatrix} M_x \\ M_y \\ M_{xy} \end{Bmatrix} = \begin{bmatrix} D_{11} & D_{12} & 0 \\ D_{12} & D_{22} & 0 \\ 0 & 0 & D_{66} \end{bmatrix} \begin{Bmatrix} \psi_{x,x} \\ \psi_{y,y} \\ \psi_{x,y} + \psi_{y,x} \end{Bmatrix} \begin{Bmatrix} Q_y \\ Q_x \end{Bmatrix} = k\begin{bmatrix} A_{44} & 0 \\ 0 & A_{55} \end{bmatrix} \begin{Bmatrix} \psi_y + w_{,y} \\ \psi_x + w_{,x} \end{Bmatrix} \tag{D2}$$

The system of linear equations of determining the unknown constants of the assumed deflection is shown as

$$-\begin{bmatrix} D_{11}\left(\frac{m\pi}{a}\right)^2 + D_{66}\left(\frac{n\pi}{b}\right)^2 + kA_{55} & (D_{12}+D_{66})\left(\frac{mn\pi^2}{ab}\right) & kA_{55}\left(\frac{m\pi}{a}\right) \\ (D_{12}+D_{66})\left(\frac{mn\pi^2}{ab}\right) & D_{22}\left(\frac{n\pi}{b}\right)^2 + D_{66}\left(\frac{m\pi}{a}\right)^2 + kA_{44} & kA_{44}\left(\frac{n\pi}{b}\right) \\ kA_{55}\left(\frac{m\pi}{a}\right) & kA_{44}\left(\frac{n\pi}{b}\right) & kA_{55}\left(\frac{m\pi}{a}\right)^2 + kA_{44}\left(\frac{n\pi}{b}\right)^2 \end{bmatrix} \begin{Bmatrix} B_{mn} \\ C_{mn} \\ A_{mn} \end{Bmatrix} = \begin{Bmatrix} 0 \\ 0 \\ P_{mn} \end{Bmatrix} \tag{D3}$$

Acknowledgments

This research is sponsored by a NASA grant under the Constellation University Institutes Project (CUIP). The program manager is Claudia Mayer at NASA John H. Glenn Research Center at Lewis Field.

References

[1] Blosser, M. L., "Advanced Metallic Thermal Protection Systems for Reusable Launch Vehicles," Ph.D. Dissertation, Mechanical and Aerospace Dept., Univ. of Virginia, Charlottesville, VA, 2000.

[2] Behrens, B., and Muller, M., "Technologies for Thermal Protection Systems Applied on Reusable Launcher," *Acta Astronautica*, Vol. 55, Nos. 3–9, Aug.–Nov. 2004, pp. 529–536.

[3] Dorsey, J. T., Poteet, C. C., Wurster, K. E., and Chen, R. R., "Metallic Thermal Protection System Requirements, Environments, and Integrated Concepts," *Journal of Spacecraft and Rockets*, Vol. 41, No. 2, March–April 2004, pp. 162–172.

[4] Blosser, M. L., "Development of Metallic Thermal Protection Systems for the Reusable Launch Vehicle," NASA TM-110296, Oct. 1996.

[5] Fung, T. C., Tan, K. H., and Lok, T. S., "Analysis of C-Core Sandwich Plate Decking," *Proceedings of the 3rd International Offshore and Polar Engineering Conference*, International Society of Offshore and Polar Engineers, Mountain View, CA, Vol. 4, 1993, pp. 244–249.

[6] Fung, T. C., Tan, K. H., and Lok, T. S., "Elastic Constants for Z-Core Sandwich Panels," *Journal of Structural Engineering*, Vol. 120, No. 10, 1994, pp. 3046–3065.

[7] Libove, C., and Hubka, R. E., "Elastic Constants for Corrugated Core Sandwich Plates," NACA TN-2289, 1951.

[8] Lok, T. S., and Cheng, Q., "Elastic Stiffness Properties and Behavior of Truss-Core Sandwich Panel," *Journal of Structural Engineering*, Vol. 126, No. 5, May 2000, pp. 552–559.

[9] Valdevit, L., Hutchinson, J. W., and Evans, A. G., "Structurally Optimized Sandwich Panels with Prismatic Cores," *International Journal of Solids and Structures*, Vol. 41, May 2004, pp. 5105–5124.

[10] Lok, T. S., Cheng, Q., and Heng, L., "Equivalent Stiffness Parameters of Truss-Core Sandwich Panel," *Proceedings of the 9th International Offshore and Polar Engineering Conference*, International Society of Offshore and Polar Engineers, Mountain View, CA, Vol. 4, 1999, pp. 292–298.

[11] Fung, T. C., Tan, K. H., and Lok, T. S., "Shear Stiffness DQy for C-Core Sandwich Panels," *Journal of Structural Engineering*, Vol. 122, No. 8, 1996, pp. 958–966.

[12] Libove, C., and Batdorf, S. B., "General Small Deflection Theory for Flat Sandwich Plates," NACA TN-1526, 1948.

[13] Tan, K. H., Fung, T. C., and Lok, T. S., "Simplified Thick Plate Analogy for the Analysis of All-Steel Sandwich Panels," *The Structural Engineer*, Vol. 71, No. 14, 2003, pp. 253–258.

[14] Vinson, J. R., *Behavior of Sandwich Structures of Isotropic and Composite Materials*, Technomic, Lancaster, PA, 1999, Chaps. 1–4.

[15] Whitney, M., *Structural Analysis of Laminated Anisotropic Plates*, Technomic, Lancaster, PA, 1987, Chaps. 7–9.

[16] Gibson, R. F., *Principles of Composite Mechanics*, McGraw–Hill, New York, 1994, Chaps. 3–6.

[17] Cook, R., and Young, W., *Advanced Mechanics of Materials*, 2nd ed., Prentice–Hall, Upper Saddle River, NJ, 1999, Chaps. 2–3.

[18] Nordstrand, T., Carlsson, L. A., and Allen, H. W., Transverse Shearing Stiffness of Structural Core Sandwich, *Composite Structures*, Vol. 27, 1994, p. 317.

[19] Hibbeler, R. C., *Mechanics of Materials*, 4th ed., Prentice–Hall, Upper Saddle River, NJ, 1999, p. 705.

A. Roy
Associate Editor